Article

Heavy-Metal Adsorption Characteristics of Scoria Distributed over the Earth Surface of Jeju Island

Soo-Hyoung Moon, Ho-Won Lee*,† and Seung-Geon Kim*

Jeju Special Self-Governing Province Development Corporation, Jeju 63345, Republic of Korea
*Department of Chemical Engineering, Jeju National University, Jeju 63243, Republic of Korea

Abstract

In this study, we investigated the various adsorption factors influencing the adsorption of heavy metal ions based on the study of the composition and physicochemical properties of scoria dispersed throughout Jeju Island. Analysis of the distribution characteristics of scoria samples collected from five areas of Jeju showed that reddish-brown-colored scoria were predominant. Analysis of scoria collected from Jeju Island showed that its mineral components are ordered as follows: $SiO_2 > Al_2O_3 > Fe_2O_3 > CaO$ and MgO. The experimental data did not show a linear relationship in the pseudo-first-order adsorption kinetics. In contrast, a pseudo-second-order model yielded a positive linear relationship, and this model was subsequently used. It could be concluded based on an intraparticle diffusion model indicating linear relationships that the capture of metal ions on scoria is dominated by the primary adsorption step.

Keywords: Scoria, Adsorption kinetic model, Heavy metal, Intraparticle diffusion

1. Introduction

Jeju Island has more than 300 small volcanic edifices (parasitic volcanoes). These are called oreums and were generated by volcanic activity on the island. The oreums are distributed over a wide area of the island. These volcanic edifices are reported to be scoria cones, cone-shaped volcanic edifices made of pyroclastic materials ejected from the volcanic crater by explosive eruptions that then accumulated around the crater[1]. The constituent material of these volcanic edifices is scoria, which is a porous pyroclastic material originating from basaltic magma. Porous scoria formed from volcanic activity has high permeability due to the many pores formed during the ejection of material during volcanic eruption. Moreover, because scoria occurs throughout the underground layers of Jeju, scoria can adsorb dissolved minerals present in the groundwater of Jeju and can also adsorb and eliminate pollutants through geochemical-water–rock reactions owing to rainwater infiltration into groundwater.

Adsorbents for the removal of pollutants from water must be inexpensive and nontoxic. Therefore, the possibility of using natural inorganic and organic geological materials as adsorbents is significant[2-5]. Recently, the possibility of using volcanic rock as an adsorbent to remove heavy metals from drinking water and wastewater has been investigated[6]. Like other volcanic rocks, scoria has a porous structure. Many studies have investigated its use in the adsorption of pollutants for application in water purification, as well as its engineering characteristics for use as a construction material[7-11].

Concerning water treatment, the most important characteristic of scoria is its porous nature, which is created when magma is ejected during a volcanic eruption and rapidly cooled. To date, studies on the adsorption characteristics of scoria regarding its porous structure are incomplete.

Hence, in this study, the physiochemical properties of scoria were characterized by carrying out physiochemical measurements on scoria samples, including specific surface area (BET) analysis, pore distribution, pore size, and surface functional group analysis. The adsorption characteristics of heavy-metal pollutants, considering the physiochemical characteristics of scoria, were also investigated. Additionally, to understand the mechanisms of pollutant adsorption in scoria, mass transfer, adsorption rate model, and intraparticle diffusion model were applied at adsorption equilibrium.

2. Experimental

2.1. Physiochemical characteristics of scoria

2.1.1. Sample selection

Scoria is abundant across Jeju Island. Therefore, studies concerning its accurate distribution and the status of deposits are less important. In this study, scoria samples were taken from the eastern and northern areas of Jeju Island, as an on-the-spot survey.

Scoria samples were collected from five locations near oreums (scoria cones) (Figure 1). The collected samples were pulverized and separated into 1.18−2.39 mm sizes, washed several times with distilled water, and dried at 95 °C for 12 h using a drying oven (DKHT con-

Figure 1. Sampling sites of scoria for test adsorbents.

vection oven) before use.

2.1.2. Analysis of sample composition

Ten mineral components were selected for analysis: SiO_2, Al_2O_3, Fe_2O_3, MgO, TiO_2, MnO, CaO, P_2O_5, K_2O, and Na_2O. The analysis was carried out by the Korea Institute of Geoscience and Mineral Resources. X-Ray fluorescence spectrometry (XRF, MXF-2400) was used for composition analysis. The chemical composition of the microelements was analyzed by decomposing the samples with heat and a mixture of acids[12]. For acid decomposition, finely pulverized scoria (0.1 g) was placed in a 50 mL Teflon beaker, mixed with a solution of HF, HNO_3, and $HClO_4$ (4:4:1 ratio), and heated to 150 °C on a hot plate for 2 h. Then, mixed acid (4 mL) was added, and the process of scoria dissolution was repeated, finally yielding white crystals. The white crystals were diluted with 3% nitric acid and were used for microelemental analysis using inductively coupled plasma optical emission spectroscopy (ICP-OES) (ICP Optical Emission Spectrometer, Varian 720-ES) and mass spectrometry (ICP-MS) (Varian 820-MS).

2.1.3. Pore structure and surface characteristics

The specific surface area of the scoria samples was analyzed using a specific surface area measurement device (BET, Nanoporosity-XQ Analyzer) at the Biomedical Nanomaterials Lab, School of Environment Science and Engineering, Pohang University of Science and Technology. Measurements were made on pulverized samples. The scoria samples were pulverized into fine powder and dried at 95 °C for 12 h for surface functional group analysis using an attenuated total reflection Fourier-transform infrared (ATR-FTIR) analyzer (Nicolet 6700, Thermo).

2.2. Adsorption experiment

2.2.1. Batch adsorption experiment

To understand the heavy-metal-adsorption characteristics of scoria, a precursor solution of heavy-metal ions (Cr^{3+}, Pb^{2+}, and Ni^{2+}) (10 mg/L) was prepared. The solution (200 mL) was poured into a 250 mL conical flask and pulverized scoria (4 g) was added. Equilibrium adsorption (mg/g) values were calculated using Eq. (1) after agitating the samples at 200 rpm and 25 °C for 24 h using a shaking incubator (HB-201SF).

$$q_e = \frac{(C_0 - C)\,V}{W} \tag{1}$$

Here, q_e is the amount of the adsorbate (mg/g) adsorbed per adsorbent gram at adsorption equilibrium, C_0 is the initial concentration (mg/L) of the adsorbate, V is the volume (L) of the solution, and W is the injected amount (g) of the adsorbent.

The adsorption characteristics were evaluated using adsorption isotherm models such as the Freundlich and Langmuir adsorption isotherm equations. These are empirical formulas representing absorptivity and are used to predict adsorption equilibrium data.

2.2.2. Adsorption Rate and Diffusion Model

To understand the rate of heavy-metal adsorption of scoria, a solution of heavy-metal ions (Cr^{3+}, Pb^{2+}, and Ni^{2+}) (10 mg/L) was produced. The solution (200 mL) was poured into a 250 mL conical flask, and scoria (4 g) was added. A shaking incubator (HB-201SF) was used to shake the samples at 200 rpm and 25 °C. Samples were shaken for 0.5, 1, 2, 3, 4, 6, 12, 18, and 24 h, and absorption was calculated per unit time. First-order adsorption rate and then second-order adsorption rate models were used for sample evaluation.

The heavy-metal adsorption rate of scoria can be treated as a mass-transfer process resulting from the adsorption process. In this study, diffusion processes were analyzed by applying the intraparticle diffusion model.

3. Results and discussion

3.1. Physiochemical characteristics of scoria

3.1.1. Chemical composition

Table 1 shows the compositions of the scoria samples. Most samples contained components in the order of $SiO_2 > Al_2O_3 > Fe_2O_3 > CaO$ and MgO, and this trend is similar to those found in a previous study on the composition of volcanic rocks[13].

The component percentage ranges of SiO_2, Al_2O_3, Fe_2O_3, CaO, and MgO were found to be 38.09~49.57 wt%, 15.71~19.11 wt%, 12.14~17.27 wt%, 5.02~9.26 wt%, and 6.23~7.34 wt%, respectively. The MnO and P_2O_5 contents were found to be lower than those of the major components.

Table 1. Bulk Chemical Composition of the Scoria Samples Determined by XRF Analysis

Sample	Major element (wt%)										
	SiO_2	Al_2O_3	Fe_2O_3	CaO	MgO	K_2O	Na_2O	TiO_2	MnO	P_2O_5	Ig. on loss
S1	38.09	19.11	17.27	5.02	7.34	0.34	1.48	3.72	0.15	0.58	6.23
S2	46.77	16.93	13.57	6.59	6.23	1.13	2.43	2.68	0.16	0.54	2.67
S3	49.57	15.94	12.14	7.62	6.39	1.74	3.10	2.39	0.16	0.54	0.11
S4	47.72	15.71	12.98	8.12	7.17	1.10	2.51	2.64	0.16	0.50	1.17
S5	47.47	16.13	12.25	9.26	7.25	1.30	2.89	2.56	0.16	0.58	0.00

Table 2. Trace Elements in the Scoria Samples

Sample	Trace elements (mg/L)								
	Li	Rb	Sb	Sr	Pb	Ge	Cu	Ni	Mo
S1	5.16±0.4	2.03 ± 1.9	< 0.5	320.98 ± 17.3	7.59 ± 1.0	< 0.5	45.61 ± 0.4	179.71 ± 0.7	41.43 ± 17.7
S2	8.33 ± 0.0	16.76 ± 2.6	< 0.5	537.43 ± 2.9	7.61 ± 2.1	< 0.5	39.56 ± 0.3	136.45 ± 0.8	25.29 ± 3.4
S3	6.99 ± 1.2	38.60 ± 4.7	< 0.5	677.50 ± 84.3	7.27 ± 0.8	< 0.5	36.15 ± 0.2	122.89 ± 0.5	45.12 ± 7.8
S4	6.72 ± 0.1	17.46 ± 0.2	< 0.5	595.87 ± 1.6	6.69 ± 0.5	< 0.5	52.64 ± 0.3	212.04 ± 0.2	14.89 ± 0.8
S5	5.86 ± 0.1	24.29 ± 1.7	< 0.5	710.47 ± 13.7	4.88 ± 1.7	< 0.5	35.66 ± 0.7	123.75 ± 0.3	12.30 ± 0.5

Sample	Trace elements (mg/L)							
	V	Zn	Zr	Se	Ba	B	As	Cr
S1	204.2 ± 3.0	175.48 ± 2.9	284.9 ± 21.8	< 0.5	240.9 ± 8.4	92.70 ± 9.65	6.4 ± 3.6	268.9 ± 4.9
S2	172.0 ± 0.8	153.49 ± 0.5	294.6 ± 1.1	< 0.5	465.4 ± 1.6	68.05 ± 0.56	7.2 ± 1.0	257.8 ± 0.3
S3	185.0 ± 1.1	151.16 ± 6.6	312.7 ± 10.8	< 0.5	458.1 ± 21.2	61.9 ± 3.09	6.43 ± 0.7	234.2 ± 2.7
S4	182.1 ± 0.3	160.6 ± 0.7	210.1 ± 1.0	< 0.5	382.5 ± 0.9	63.6 ± 0.3	6.7 ± 1.6	197.7 ± 0.6
S5	213.4 ± 0.2	129.6 ± 0.6	187.9 ± 7.7	< 0.5	379.6 ± 8.9	56.6 ± 0.6	3.7 ± 0.3	262.5 ± 0.6

The results of microelemental analysis using the acid decomposition method are shown in Table 2. Among the microelements, Sb, Ge, and Se contents in scoria were found to be very low (mostly showing values below the detection limit (< 0.5 mg/L)); in contrast, Sr, Zr, Ba, Zn, and V contents were found to be relatively high.

3.1.2. Petrologic classification

To classify and name the scoria samples, the IUGS classification map using the total alkali (Na_2O + K_2O) − SiO_2 and the alkaline and subalkaline series classification maps were used (Figure 2).

The alkali content (Na_2O + K_2O) of scoria correlated positively with increasing SiO_2 content. Petrologic classification confirmed that the scoria mostly comprised basalt and trachybasalt. For series classification, we confirmed that all scoria samples analyzed could be classified into the alkali rock series.

3.2. Pore structure and characteristics

3.2.1. Measurement of the specific surface area

Nitrogen adsorption isotherms were used to investigate the effects of pore characteristics on the pollutant adsorption characteristics of scoria, and the BET equation was used to interpret the results (Figure 3). The specific surface area of scoria was found to be between 30.0 and 177.5 m^2/g. The highest surface area, 177.5 m^2/g, was found for the light-
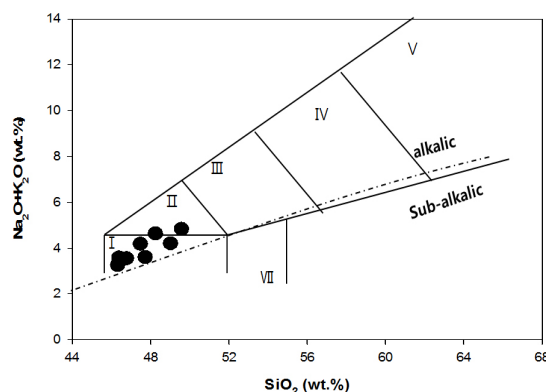
Figure 2. (Na_2O + K_2O) vs. SiO_2 plot of the scoria. Solid line: I-basalt; II-trachybasalt; III-basaltic trachyandesite; IV-trachyandesite; V-trachyte; VII-basaltic andesite. Dotted-line: Boundary between alkaline and subalkaline series.

brown samples taken from the Dunji oreum (S1), and the lowest (30.7 m^2/g) was found for the sample collected at the Yongnuni oreum.

3.2.2. Pore characteristics

In some cases, the adsorption capacities of the scoria did not relate with total pore area. Consequently, we evaluated the porosity of scoria
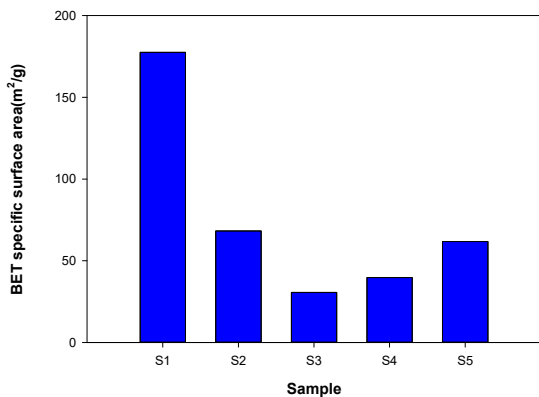
Figure 3. BET specific surface area (m²/g) of the scoria samples.

by analyzing the pore distribution, which is a key factor in determining porosity.

In this study, the mesopore and micropore volumes were measured using the nitrogen adsorption method. The Barrett-Joyner-Halenda (BJH) method was used to evaluate the mesopore volume, and the Horvath and Kawazoe (HK) method was used to evaluate the micropore volume.

Of the samples analyzed, most had pore size lower than 200 Å. In particular, scoria from the Dunji oreum (S1) had the highest specific surface area, and the pore volume was shown to be highly developed with pore diameters of less than 200 Å. According to Allen, huge pores with diameters greater than 500 Å act as passages to the meso and micropores and do not significantly affect the surface area of the adsorbent[13]. Accordingly, most pores less than 200 Å, except huge pores, are predicted to affect the adsorptive power of the scoria.

Micropore volume was measured for pore diameters less than 20 Å,

confirming that micropores less than 20 Å were found from all scoria samples. In particular, micropores with diameters less than 10 Å were found to be more developed in scoria from the Dunji oreum, with comparatively larger specific surface areas. This demonstrates that scoria micropores have a significant effect on the specific surface area.

The mean mesopore and micropore diameters were measured, and the results are shown in Table 3. The mesopore diameters were between 35.56 and 42.41 Å, a relatively wide range. The micropore diameters were in the range of 12.97−14.34 Å. Of the scoria samples, the mean micropore diameter of the Dunji oreum scoria was found to be the smallest, 12.97 Å. However, the mean mesopore pore diameter this sample was not the smallest compared to other scorias. Consequently, there is no perfect correlation between the mean pore diameters of the mesopores and micropores.

3.3. Adsorption characteristics

3.3.1. Adsorption isotherm

We used adsorption isotherm models to predict adsorption equilibrium data; for example, using empirical formulas that yield information on the adsorption characteristics. The results of measurements are shown in Table 4. The adsorption isotherm for lead cations (Pb^{2+}) could not be adequately measured. Thus, adsorption model equations were applied to chromium (Cr^{3+}) and nickel (Ni^{2+}) ions. The suitability of two adsorption isotherms, Langmuir and Freundlich, was assessed using the correlation coefficient (R^2). High correlation coefficients were found when using the Freundlich adsorption isotherm, indicating that this isotherm is more appropriate to analyze adsorption in scoria. In addition, the Freundlich adsorption isotherm had a better linear relationship than that of the Langmuir adsorption isotherm, as shown in Figures 4 and 5.

Table 3. Comparison between Mean Mesopore Diameter and Mean Micropore Diameter

Item	S1	S2	S3	S4	S5
Mean micro pore diameter (Å)	12.97	14.17	13.47	13.99	14.34
Mean Meso pore diameter (Å)	35.56	38.18	39.32	35.74	42.41

Table 4. Evaluation of Applicability of the Langmuir and Freundlich Adsorption Isotherms to the Adsorption of Heavy Metals by Scoria

Sample	Heavy metal	Langmuir isotherm	Freundich isotherm		
		Correlation coefficient (r^2)	Correlation coefficient (r^2)	K	1/n
S1	Cr^{3+}	0.881	0.816	0.156	0.400
	Ni^{2+}	0.456	0.820	0.165	0.321
S2	Cr^{3+}	0.951	0.943	0.184	0.415
	Ni^{2+}	0.770	0.846	0.184	0.353
S3	Cr^{3+}	0.590	0.616	0.563	0.116
	Ni^{2+}	0.744	0.788	0.336	0.306
S4	Cr^{3+}	0.574	0.844	0.148	0.412
	Ni^{2+}	0.952	0.979	0.150	0.427
S5	Cr^{3+}	0.549	0.255	0.310	0.276
	Ni^{2+}	0.805	0.845	0.185	0.366
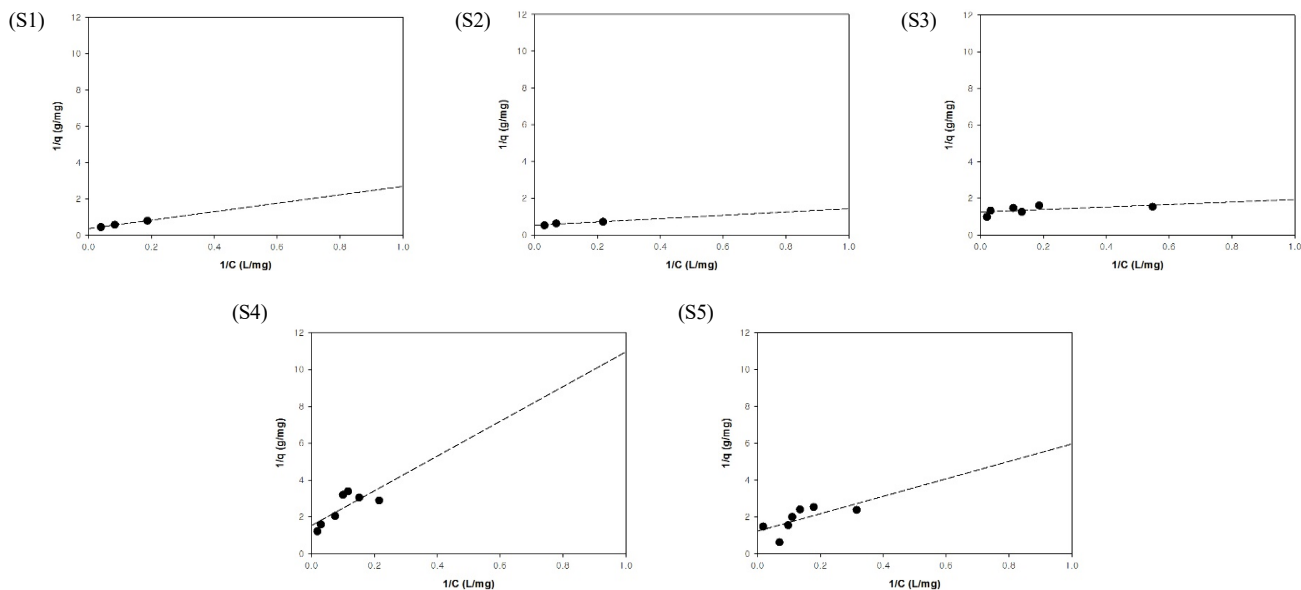
Figure 4. Distribution of Cr^{3+} ions between the adsorbent and aqueous phases. The dashed line represents the Langmuir isotherm.
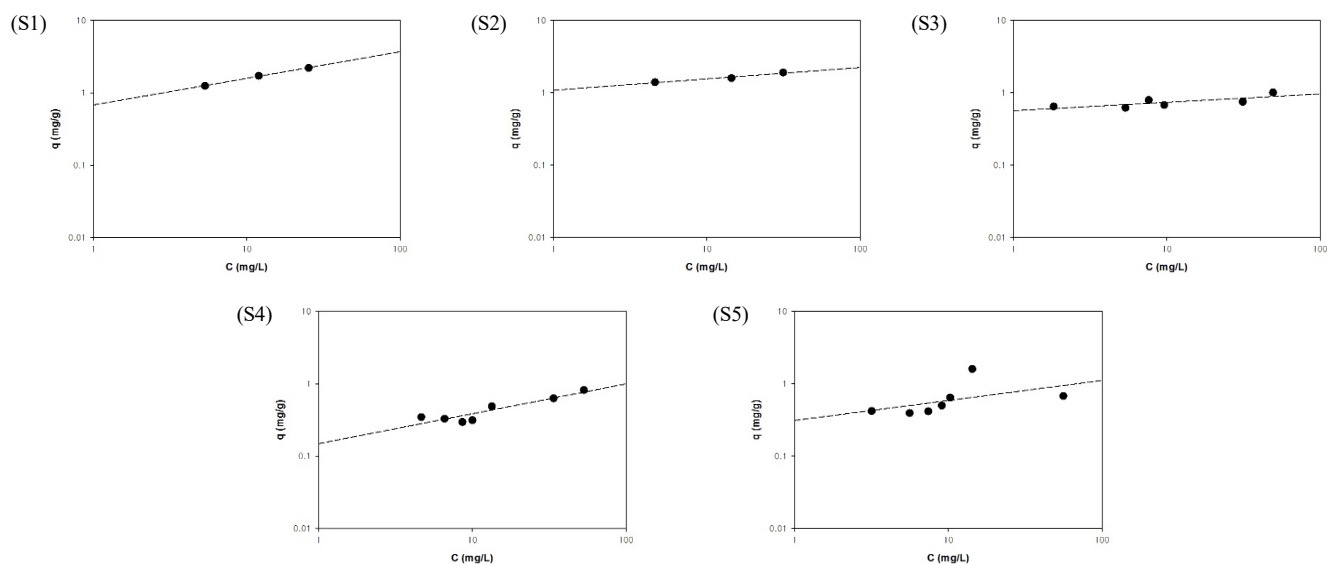
Figure 5. Distribution of Cr^{3+} ions between the adsorbent and aqueous phases. The dashed line represents the Freundlich isotherm.

3.3.2. Adsorption capacity

The equilibrium adsorption values for Cr^{3+} was the highest, lying between 0.34 and 0.50 mg/g, and was 0.50 mg/g in samples S1 and S2, showing no significant difference between these samples despite having the highest equilibrium adsorption value. The equilibrium adsorption value of Pb^{2+} was higher than those of the other heavy metals, at 0.48~0.50 mg/g. Equilibrium adsorption values for divalent nickel ions (Ni^{2+}) were between 0.22 and 0.45 mg/g, and there were differences between S1 and S2, samples that had similar adsorption values for trivalent chromium ion (Cr^{3+}). The high adsorption capacity of S1 and S2 was measured in samples with high specific surface area values.

3.3.3. Adsorption rate model

First-order and second-order adsorption models were used to analyze

Table 5. Amount of Heavy Metal Adsorbed onto Scoria at Equilibrium

Sample	q_e (mg/g)		
	Cr^{3+}	Pb^{2+}	Ni^{2+}
S1	0.50	0.50	0.43
S2	0.50	0.50	0.45
S3	0.47	0.50	0.33
S4	0.46	0.48	0.22
S5	0.34	0.48	0.24

the adsorption rate of the scoria samples (Figures 6 and 7). No perfect linear relationship was found for the majority of scoria samples. The R^2 values fitted from the trend line on applying the adsorption rate model equation are listed in Table 6.

Table 6. Rate Constants and q_e Calculated from the First-order and Second-order Rate Equations for Sorption of Heavy Metals onto Scoria

Sorbent	Sorbate	Pseudo-first order		Pseudo-second order			Experimental
		k_1	R^2	k_1	R^2	q_e (mg/g)	q_e (mg/g)
S1	Cr^{3+}	0.006	0.7599	0.05	0.9973	0.52	0.50
	Pb^{2+}	0.004	0.4198	5.82	1.000	0.50	0.50
	Ni^{2+}	0.007	0.9885	0.09	0.9993	0.43	0.43
S2	Cr^{3+}	0.0054	0.8137	0.0837	0.9993	0.507	0.497
	Pb^{2+}	0.0047	0.6275	2.147	1.000	0.499	0.499
	Ni^{2+}	0.0043	0.8937	0.1470	0.9998	0.449	0.445
S3	Cr^{3+}	0.0035	0.9672	0.0012	0.9859	0.495	0.478
	Pb^{2+}	0.0015	0.1750	0.0395	0.9998	0.496	0.499
	Ni^{2+}	0.0022	0.7547	0.0011	0.9978	0.331	0.333
S4	Cr^{3+}	0.0033	0.8947	0.0023	0.9981	0.487	0.476
	Pb^{2+}	0.0041	0.5625	0.0368	1.000	0.482	0.482
	Ni^{2+}	0.006	0.9099	0.001	0.9997	0.226	0.223
S5	Cr^{3+}	0.0019	0.9736	0.00023	0.9611	0.367	0.341
	Pb^{2+}	0.0065	0.6472	0.0698	1.000	0.479	0.478
	Ni^{2+}	0.0019	0.5937	0.0003	0.9901	0.234	0.238
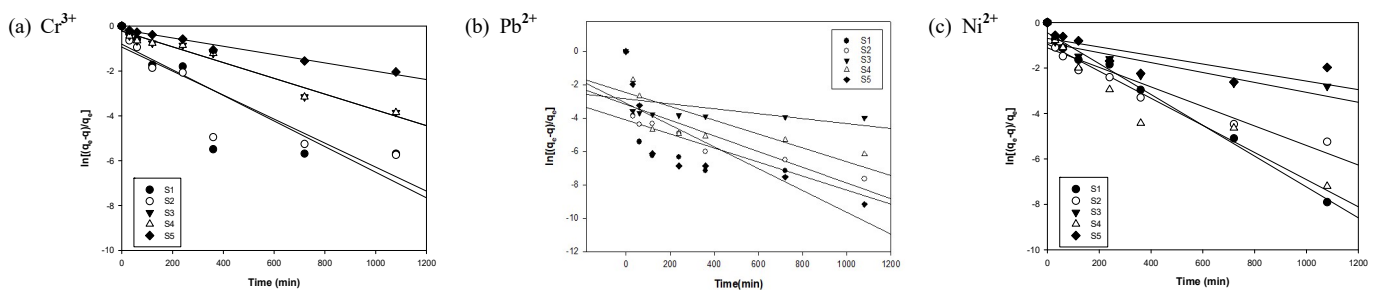
Figure 6. Plots of pseudo-first-order adsorption kinetic models; (a) Cr^{3+}, (b) Pb^{2+}, (c) Ni^{2+}.
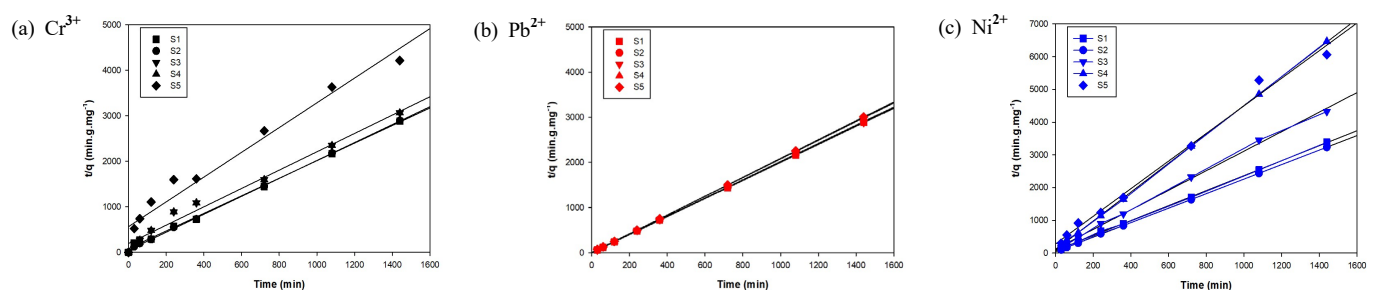
Figure 7. Plots of pseudo-second-order adsorption kinetic models; (a) Cr^{3+}, (b) Pb^{2+}, (c) Ni^{2+}.

These results indicated that the adsorption of metal ions in scoria is not first order. The R^2 values for the adsorption of Cr^{3+}, Pb^{2+}, and Ni^{2+} were measured to be between 0.7599 and 0.9736, 0.1750 and 0.6472, and 0.5937 and 0.9885, respectively.

The second-order adsorption model assumes that the rate-limiting step is chemical adsorption accompanied by an electron transfer between the adsorbent and the adsorbate; for example, electron exchange or the formation of a covalent bond between the adsorbent and the ad-

sorbate[14]. The second-order adsorption model can be divided into two steps. An initial step, in which the solute-removal rate increases rapidly on initial contact between the solution and the solid material (scoria), and a second stage, in which the rate of solute removal slowly increases until equilibrium is reached. In Figure 7, the result of application of second-order kinetics is shown; a good linear relation was observed for all scoria samples when plotting t/q against time, t. Consequently, to model the adsorption of metal ions in scoria, a sec-
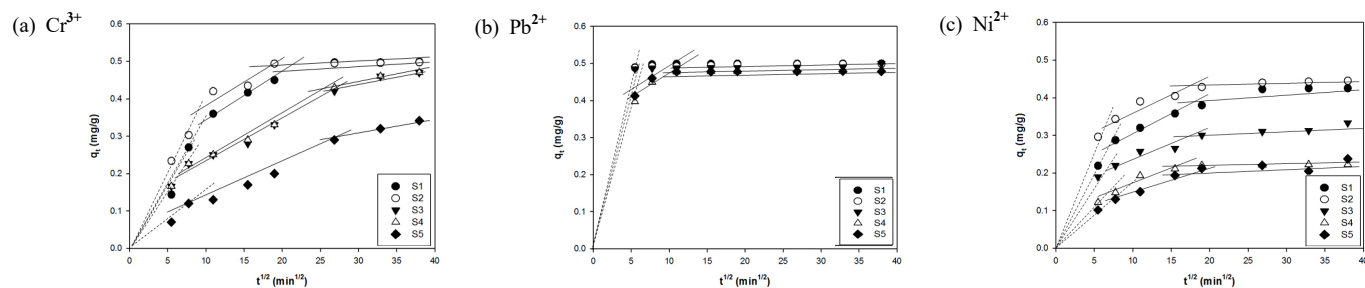
Figure 8. Intraparticle diffusion kinetics for the adsorption of scoria; (a) Cr^{3+}, (b) Pb^{2+}, (c) Ni^{2+}.

Table 7. Parameters of Intraparticule Diffusion Model

Sample	Sorbate	First linear part	Second linear part		Third linear part	
		k_1 $(mg \cdot g^{-1} \cdot min^{-1/2})$	k_2 $(mg \cdot g^{-1} \cdot min^{-1/2})$	R^2	k_3 $(mg \cdot g^{-1} \cdot min^{-1/2})$	R^2
S1	Cr^{3+}	0.0333	0.0085	0.9641	0.0001	0.7063
	Pb^{2+}	0.0894	0.0001	0.8252	4×10^{-5}	0.9970
	Ni^{2+}	0.0376	0.0064	0.9875	0.0002	0.8182
S2	Cr^{3+}	0.0398	0.0089	0.8414	0.0002	0.9674
	Pb^{2+}	0.0887	0.0003	0.8395	5×10^{-5}	0.7913
	Ni^{2+}	0.0461	0.0032	0.9155	0.0005	0.9998
S3	Cr^{3+}	0.0294	0.0099	0.9516	0.0	1.000
	Pb^{2+}	0.0887	0.0002	0.9473	3×10^{-5}	0.7467
	Ni^{2+}	0.0295	0.0036	0.8540	0.0009	0.8051
S4	Cr^{3+}	0.0297	0.0098	0.9120	0.0018	0.9976
	Pb^{2+}	0.0725	0.0023	0.5978	0.0002	0.9978
	Ni^{2+}	0.0197	0.0017	0.7181	0.0002	0.8539
S5	Cr^{3+}	0.0150	0.0087	0.9984	0.0009	0.7063
	Pb^{2+}	0.0753	0.0058	0.6733	3×10^{-5}	0.7913
	Ni^{2+}	0.0171	0.0042	0.7868	0.0008	0.9123

ond-order model was used, and the R^2 values for Cr^{3+}, Pb^{2+}, and Ni^{2+} were found to be between 0.9611 and 0.9993, 0.9998 and 1.0000, and 0.9901 and 0.9998, respectively. Furthermore, the theoretical adsorption equilibrium value (q_e), obtained from the straight line of the second adsorption rate equation, and the equilibrium adsorption (q_e), obtained from experiment, corresponded almost exactly to each other.

Kim et al.[7] revealed that the main functional groups that exist on the surface of scoria are Si-O-M^+ (M^+ = metal ions). Consequently, Cr^{3+}, Pb^{2+}, and Ni^{2+} ions are thought to be involved in the chemical adsorption reactions accompanied by chemical bond formation or ion reactions with Si-O-M^+ on the scoria surface in the form of functional groups.

3.3.4. Internal diffusion model

Adsorption processes are governed by several steps. These steps can be divided into the diffusion of the solute into the solution over the boundary layer around the particles, the diffusion from the boundary layer to the surface of the particles (external diffusion), the diffusion from the surface into the internal area (pore diffusion or surface diffusion), and the adsorption step accompanied by physiochemical adsorption[15,16]. Because the adsorption characteristics of the diffusion

mechanism cannot be evaluated using a first- or second-order adsorption model, we analyzed the diffusion process using the intraparticle diffusion model proposed by Weber et al.[17].

Adsorption experiments were carried out by agitating the solutions at 200 rpm. The results of applying the intraparticle diffusion model to the adsorption processes in scoria are shown in Figure 8. The straight lines can be divided into three areas: the first straight line represents fast adsorption when the solution of heavy-metal ions is diffusing over the boundary layer and, then, from the boundary layer to the particle surface. The second straight line is related to diffusion within the pores. The third straight line represents intraparticle diffusion. At this stage, the concentration of the remaining heavy-metal ions, the adsorbate, is very low, and the diffusion speed decreases. This result is similar to those of previously reported adsorption studies[18-20].

Table 7 shows the reaction rate constants derived from the three straight-line areas. That of the first straight line (first step), involved in fast adsorption reactions, is greater than those of the second and third straight lines (second and third steps).

On applying the adsorption rates obtained to the diffusion model, the fast adsorption step at the beginning of the adsorption was shown to be due to external diffusion of the heavy-metal ions. Adsorption repre-

sented by the second and third straight line areas is the slow adsorption reaction: intraparticle diffusion, i.e., internal diffusion. We confirmed that the rate-determining step is that at which diffusion inside the pores governs the adsorption rate.

4. Conclusions

We investigated the chemical composition and physiochemical characteristics of scoria distributed over Jeju Island. We also investigated the various adsorption factors affecting heavy-metal-ion absorption on scoria could be conclusively summarized as :

1. The principle components of scoria may be ordered as such SiO_2 > Al_2O_3 > Fe_2O_3 > CaO and MgO, and scoria was classified in the alkali rock series, which includes basalt and trachyandesite.

2. The specific surface areas of the samples were analyzed, and were found to be between 30.0 and 177.6 m^2/g. Micropore volumes were measured for pore diameters of less than 20 Å, and the presence of micropores in the scoria samples was confirmed.

3. Several adsorption rate models were applied to the data. Although no perfect linear relationship was found for the first-order adsorption model, a good linear relation was found for the second-order adsorption rate model. In addition, the internal diffusion model was applied, and three straight-line plots were obtained. Fast adsorption occurs at the beginning of the adsorption, which is an external diffusion step. The second and third straight lines represent slow adsorption reactions. Intraparticle diffusion, which is internal diffusion, is a slow step. We confirmed that, concerning adsorption in scoria, intraparticle diffusion is the rate-determining step, governing the adsorption rate.

Acknowledgement

References

1. J. H. Lee and S. H. Yun, Morphological analysis of quternary monogenetic volcanoes in Jeju island, Korea, *J. Geol. Soc. Korea*, **48**, 383-400 (2012).

2. C. H. Jeong and G. Y. Jeong, Effect of groundwater anions and pH on the sorption removal of heavy metals by bentonite, *Econ. Environ. Geol.*, **33**, 31-40 (2000).

3. U. Wingenfelder, C. Hansen, G. Furrer, and R. Schulin, Removal of heavy metals from mine waters by natural zeolites, *Environ. Sci. Technol.*, **39**, 4606-4613 (2005).

4. M. G. Fonseca, M. M. Oliveira, and L. N. H. Arikaki, Removal of cadmium, zinc, manganese and chromium cations from aqueous solution by a clay mineral, *J. Hazard. Mater.*, **B137**, 288-292 (2006).

5. J. H. Potgieter, S. S. Potgieter-Vermaak, and P. D. Kalibantona, Heavy metals removal from solution by palygorskite clay, *Miner. Eng.*, **19**, 463-470 (2006).

6. M. Yavuz, F. Gode, E. Pehlivan, S. Ozmert, and Y. C. Sharma, An economic removal of Cu^{2+} and Cr^{3+} on the new adsorbents: Pumice and polyacrylonitrile/pumice composite, *Chem. Eng. J.*, **137**, 453-461 (2008).

7. S. G. Kim, S. H. Moon, and H. W. Lee, Adsorption behavior of heavy metals and organics in the mixed packed column of socria/activated carbon, *Appl. Chem. Eng.*, **32**, 97-101 (2021).

8. J. S. Kwon, S. T. Yun, S. O. Kim, B. Mayer, and I. Hutcheon, Sorption of Zn(II) in aqueous solutions by scoria, *Chemosphere*, **60**, 1416-1426 (2005).

9. J. M. Morgan-Sagastume and A. Noyola, Evaluation of an aerobic submerged filter packed with volcanic scoria, *Bioresour. Technol.*, **99**, 2528-2536 (2008).

10. E. Alemayehu and B. Lennartz, Virgin volcanic rocks : Kinetics and equilibrium studies for the adsorption of cadmium from water, *J. Hazard. Mater.*, **169**, 395-401 (2009).

11. S. H. Moon, H. W. Lee, J. H. Kim, K. K. Kang, and Y. S. Mok, Characteristics of volcanic cinders and their adsorption trait for heavy metal removal, *Res. J. Chem. Environ.*, **15**, 920-927 (2011).

12. M. S. Choi, C. S. Cheong, and K. H. Park, An experimental study on the trace element analysis of rock samples with regard to the decomposition method, *J. Petrol. Soc. Korea*, **3**, 41-48 (1994).

13. T. Allen, *Particle Size Measurement*, 4th ed., Champman & Hall, NY, USA (1990).

14. Y. S. Ho and G. McKay, Pseudo-second order model for sorption processes, *Process Biochem.*, **34**, 451-465 (1999).

15. Ö. Gerçel, A. Özcan, A. S. Özcan, and H. F. Gerçel, Preparation of activated carbon from a renewable bio-plant of Euphorbia rigida by H_2SO_4 activation and its adsorption behavior in aqueous solutions, *Appl. Surf. Sci.*, **253**, 4843-4852 (2007).

16. F. C. Wu, R. I. Tseng, and R. S. Juang, Kinetic modeling of liquid-phase adsorption of reactive dyes and metal ions on chitosan, *Water Res.*, **35**, 613-618 (2001).

17. W. J. Weber and J. C. Morris, Kinetics of adsorption on carbon from solution, *J. Sanit. Eng. Div., Am. Soc. Civ. Eng.*, **89**, 31-60 (1963).

18. P. S. Kumar, Removal of Congo red from aqueous solutions by neem saw dust carbon, *Colloid J.*, **72**, 703-709 (2010).

19. T. S. Singh and K. K. Pant, Kinetics and mass transfer studies on the adsorption of arsenic onto activated alumina and iron oxide impregnated activated alumina, *Water Qual. Res. J. Canada*, **41**, 147-156 (2006).

20. M. Toor and B. Jin, Adsorption characteristics, isotherm, kinetics, and diffusion of modified natural bentonite for removing diazo dye, *Chem. Eng. J.*, **187**, 79-88 (2012).

Authors

Soo-Hyoung Moon; Ph.D., Chief Researcher, Jeju Special Self-Governing Province Development Corporation, Jeju 63345, Republic of Korea; justdoit74@jpdc.co.kr

Ho-Won Lee; Ph.D., Professor, Department of Chemical Engineering, Jeju National University, Jeju 63243, Republic of Korea; hwlee @jejunu.ac.kr

Seung-Geon Kim; Ph.D., Lecturer, Department of Chemical Engineering, Jeju National University, Jeju 63243, Republic of Korea; jyushin @jejunu.ac.kr